Spin-Density Functionals of a Two-Dimensional Fermionic Gas of Dipolar Atoms: Thomas-Fermi-Dirac Treatment

Fang Yiyuan
(BSc. (Hons.), NUS)
HT081313B

Supervisor: Professor B.-G. Englert

A THESIS SUBMITTED

FOR THE DEGREE OF MASTER OF SCIENCE
DEPARTMENT OF PHYSICS
NATIONAL UNIVERSITY OF SINGAPORE

2010

Acknowledgments

I would like to express my deepest gratitude towards my supervisor, Professor B.-G. Englert, for his guidance in physics and beyond. Learning from and working with him has been an invaluable experience for me.

I would also like to thank Benoît Grémaud, Christian Miniatura, Kazimierz Rzążewski for their stimulating discussions in related areas and their intriguing ideas in the subject matter.

This project is supported by Centre for Quantum Technologies, a Research Centre of Excellence funded by Ministry of Education and National Research Foundation of Singapore.

Contents

List of Tables **5**

List of Figures **6**

List of Symbols **7**

1 Introduction **11**

2 Density Functional Theory: a brief overview **13**

3 The spin-polarized case in 2D **15**

3.1 Into the flatland 15

3.2 Thomas-Fermi-Dirac approximation 16

3.3 The 2D functionals for a spin-polarized system 17

3.4 Dimensionless variables 18

4 The spin-dependent formalism **22**

4.1 Wigner function with spin-dependence 22

4.2 Extending Dirac's approximation 24

4.3 The spin-density functionals 26

4.4 A constant magnetic field 31

4.5 The weakly-interacting limit 33

4.6 Arbitrary direction of polarization 34

5 Concluding remarks and outlook **36**

A Dipole-dipole interaction in a one-dimensional spin-polarized system **40**

B A short review of concurrent works **44**

Summary

In this thesis, the spin-density functionals are derived for the ground-state energies of a two-dimensional gas of neutral atoms with magnetic-dipole interaction, in the Thomas-Fermi-Dirac approximation. For many atoms in a harmonic trap, we discuss the numerical procedures necessary to solve for the single-particle density and spin-imbalance density, in dependence on the interaction strength and the external magnetic field. We also give analytical solutions in the weak-interaction limit that is relevant for experiments.

List of Tables

A.1 Summary of the density functionals for the kinetic and interaction energy in 1D, 2D, and 3D. 43

List of Figures

3.1 The dimensionless single-particle spatial density of a spin-polarized system in dependence on the interaction strength. 20

4.1 $f(\gamma)$ at relevant values of γ. 29

4.2 $\chi(y)$ and the relative error of $y^2 \approx \chi(y)$ at relevant values of y. 30

4.3 The dimensionless single-particle spatial density of a spin mixture. . . . 34

A.1 An illustration of a 1D spin-polarized cloud of dipolar atoms. 41

List of Symbols[1]

$\frac{1}{2}M\omega^2R^2$	chemical potential for the spin-polarized case	18
$\frac{1}{2}X^2$	dimensionless Lagrange multiplier	31
A	$\equiv \frac{v_0}{\hbar\omega}\frac{1}{\sqrt{N}}$	31
a	natural length scale of our system	18
α	azimuthal angle of $\boldsymbol{\mu}$	41
$\alpha_m,\ \beta_m$	components of $\phi_m r_j$	24
$\mathbf{B}(\mathbf{r})$	external magnetic field with position dependence	22
$B(\mathbf{r})$	the magnitude of the external magnetic field	22
B_0	constant magnitude of magnetic field	31
C	$\equiv \frac{3e_{0,z}^2-1}{2}\frac{256}{45}\sqrt{\pi}$	31
Cr	Chromium	35
$\cos\big(\vartheta(\mathbf{x})\big)$	fractional spin-imbalance density	29
E	energy	*
$E_{\rm dd}$	dipole-dipole interaction energy	17
$E_{\rm dd,s}$	singlet dipole-dipole interaction energy	27
$E_{\rm kin}$	kinetic energy	17
$E_{\rm mag}$	magnetic energy	26
$E_{\rm TFD}^{(\rm 2D)}$	total energy of a 2D system under TFD treatment	19
$E_{\rm trap}$	trap energy	17
$E(\ )$	the complete elliptic integral of the second kind	28

[1]The page where a given symbol are defined/introduced is listed at the rightmost column. When the definition is general, page number is given as*.

Erfc()	complementary error function	42
$\mathbf{e}(\mathbf{r})$	the direction of the external magnetic field	22
$e_z(\mathbf{r})$	z-component of $\mathbf{e}(\mathbf{r})$	28
$\mathbf{e}_0$	constant direction of magnetic field	31
$e_{0,z}$	z-component of $\mathbf{e}_0$	31
ϵ	dimensionless interaction strength	19
f	$\equiv (\gamma^{-1} + 14 + \gamma)E(\gamma) + (-\gamma^{-1} - 6 + 7\gamma)K(\gamma)$	28
$\tilde{f}(\gamma)$	$\equiv \frac{15}{4}\pi + (16 - \frac{15}{4}\pi)\gamma$	28
ϕ	polar angle of mbr	41
$\phi_m(r_j)$	spin-dependent single-particle orbital	24
φ	polar angle of $\boldsymbol{\mu}$	41
$g(\mathbf{x})$	dimensionless single-particle spatial density	18
γ	$\equiv (P_-(\mathbf{r})/P_+(\mathbf{r}))^2$, ratio of Fermi energies	28
H	Hamilton operator	*
$\mathbf{h}(\mathbf{x})$	$\equiv h(\mathbf{x})\mathbf{e}(\mathbf{x})$	29
$h(\mathbf{x})$	dimensionless single-particle spin-imbalance density	29
$\hbar$	Planck's constant divided by 2π	*
$\eta(\ )$	Heaviside unit step function	17
$K(\ )$	the complete elliptic integral of the first kind	28
k_B	Boltzmann's constant	*
l_0	transverse harmonic oscillator length scale	19
l_z	harmonic oscillator length scale in the z-direction	15
M	mass of a single atom	*
$\boldsymbol{\mu}$	magnetic dipole moment of an atom	19
μ	magnitude of the magnetic dipole of an atom	18
μ_0	permeability of free space	18
N	number of atoms/particles	*
$n(\mathbf{r})$	single-particle spatial density	13

$n_\perp(\mathbf{r}_\perp)$ single-particle spatial density in 2D 16

$n^{(1)}(\mathbf{r}';\mathbf{r}'')$ single-particle spatial density matrix 16

$n_\perp^{(1)}(\mathbf{r}'_\perp;\mathbf{r}''_\perp)$ single-particle spatial density matrix in 2D 16

$\underline{n}(\mathbf{r}';\mathbf{r}'')$ spin-dependent single-particle spatial density matrix 25

$n^{(2)}(\mathbf{r}'_1,\mathbf{r}'_2;\mathbf{r}''_1,\mathbf{r}''_2)$ two-body spatial density matrix in 3D 17

$\underline{\underline{n}}^{(2)}(\mathbf{r}'_1,\mathbf{r}'_2;\mathbf{r}''_1,\mathbf{r}''_2)$ spin-dependent two-body spacial density matrix 25

$\nu(\mathbf{r},\mathbf{p})$ single-particle Wigner function in 3D 15

$\nu_\perp(\mathbf{r}_\perp,\mathbf{p}_\perp)$ single-particle Wigner function in 3D 15

$\underline{\nu}(\mathbf{r},\mathbf{p})$ spin-dependent single-particle Wigner function 23

ω angular frequency of the harmonic confinement in 2D or 3D .... *

ω_z angular frequency of the axial harmonic confinement 15

$P_\pm(\mathbf{r})$ radii of Wigner function of the two spin components 23

$\mathbf{p}$ momentum vector in 2D or 3D ..... *

$\mathbf{p}_\perp$ momentum vector in 2D 15

p_z axial momentum 15

θ azimuthal angle of $\mathbf{r}$ 43

R_{TF} Thomas-Fermi radius 31

$\mathbf{r}$ position vector in 2D or 3D ..... *

$\mathbf{r}_\perp$ position vector in 2D 15

$\boldsymbol{\rho}$ $\equiv \mathbf{r}' - \mathbf{r}''$, relative coordinate in 2D 28

$\rho(\mathbf{p})$ single-particle momentum distribution 16

$\rho_\perp(\mathbf{p}_\perp)$ single-particle momentum distribution in 2D 16

ϱ polar radius of $\mathbf{r}$ 41

$s(\mathbf{r})$ single-particle spin-imbalance density 24

$\boldsymbol{\sigma}$ Pauli vector of a single dipole 23

T temperature ..... *

t $\equiv |z - z'|/(\sqrt{2}l_0)$ 42

$\boldsymbol{\tau}$ Pauli vector of a second dipole 28

$V(\mathbf{r})$	position dependent external potential 13
$V_{\mathrm{dd,t}}(\mathbf{r})$	triplet dipole-dipole interaction potential 42
v_0	$\equiv B_0\mu$ 31
$\mathbf{x}$	dimensionless position variable in 2D 18
x_-	radius of the spin mixture 33
x_+	radius of the entire cloud 33
$\chi(y)$	$\equiv \frac{1}{2^{5/2}}\Big((1+y)^{5/2}+(1-y)^{5/2}-\frac{1}{8}f\big(\frac{1-y}{1+y}\big)(1+y)^{3/2}(1-y)\Big)$ 30
$\psi(r_1,\cdots,r_N)$	ground-state many-body wave function of a N-fermion system 24
z	axial position 15
z_+	$\equiv \frac{1}{2}(z'+z'')$, centre of mass coordinate 16
z_-	$\equiv z'-z''$, relative coordinate 16
$-\zeta$	chemical potential for the spin-mixture case 23

Chapter 1

Introduction

It is now well-known that certain condensed-matter phenomena can be reproduced by loading ultra-cold atoms into optical lattices [1, 2], with an advantage that the relevant parameters, such as configuration and strength of potential, interatomic interaction and so on, can be accurately controlled, while ridding spurious effects that destroy quantum coherence. In the local group, the perspective experiment to study the behaviour of ultra-cold fermions in the honeycomb lattice has initiated theoretical studies of the system. As part of this activity, this thesis focuses on the collective behaviour of fermions with magnetic-dipole interaction, confined in a two-dimensional (2D) harmonic potential.

Density functional theory (DFT), first formulated for the inhomogeneous electronic gas [3], is in fact valid generally for a system of interacting particles under the influence of an external potential, provided that the ground state is not degenerate [4], which is not a serious constraint for practical applications. While the formalism itself can be applied to both the spatial [3] and the momental density [5], the spatial-density formalism gives a more natural description in the case of a position-dependent interaction, such as the magnetic dipole interaction. We derive the density functionals and investigate the ground-state density and energy of the system.

The thesis is organized as follows. Chapter 2 gives a brief overview of ideas behind DFT that is relevant to our calculation. In Chap. 3, we review the results for our earlier

work on the density functional for the ground-state energy of a 2D, spin-polarized (SP) gas of neutral fermionic atoms with magnetic-dipole interaction, in the Thomas-Fermi-Dirac (TFD) approximation. This formalism is then generalized to a system allowing a spin-mixture (SM), Chap. 4, where the spin-density functional is derived and numerical procedures to solve for the single-particle spatial density is outlined. We conclude with a summary and a brief outline of prospective work in Chap. 5. The mathematical procedures to derive an expression for the interaction energy for a one-dimensional (1D) system is reproduced in Appendix A, and a review of other research projects of the candidate is included as Appendix B.

Chapter 2

Density Functional Theory: a brief overview

Before presenting this work, which is based on DFT, it is helpful to briefly outline the ideas relevant to our application.

The basic concept behind DFT is simple yet elegant. It states that the ground state properties of a system of many particles subjected to an external potential is a functional of the single-particle density, which is treated as the basic variable function [3]. The statement was soon shown to be valid for interacting system with an effective single-particle potential in the equivalent orbital description [6].

For any state $|\ \rangle$ of a system of N identical particles, the single-particle spatial density is defined as

$$n(\mathbf{r}) = N \int (d\mathbf{r}_2) \cdots (d\mathbf{r}_N) \left| \langle \mathbf{r}, \mathbf{r}_2, \cdots, \mathbf{r}_N | \ \rangle \right|^2, \tag{2.1}$$

where the $\mathbf{r}_i$ denotes the position of the i^{th} particle and $(d\mathbf{r}_i)$ denotes the corresponding volume element. The pre-factor, N, arises from the fact that the wave function is properly symmetrized.

Suppose two different external potentials $V_{1,2}(\mathbf{r})$ applied to the same system give identical ground-state single-particle density, $n(\mathbf{r})$, one could find the ground-state energy

for each potential,

$$E_1 = \langle 1|H_1|1\rangle < \langle 2|H_1|2\rangle = E_2 + \int (d\mathbf{r})\,(V_1(\mathbf{r}) - V_2(\mathbf{r}))\,n(\mathbf{r})\,,$$

$$E_2 = \langle 2|H_2|2\rangle < \langle 1|H_2|1\rangle = E_1 + \int (d\mathbf{r})\,(V_2(\mathbf{r}) - V_1(\mathbf{r}))\,n(\mathbf{r})\,, \tag{2.2}$$

where $H_{1,2} = H_{\rm kin} + \sum_{j=1}^{N} \left(V_{\rm int}(\mathbf{r}_j) + V_{1,2}(\mathbf{r}_j)\right)$ are the Hamilton operators, being the sum of the kinetic, effective interaction, and potential terms, and $|1\rangle$, $|2\rangle$ are the respective ground states. The sum of the above equation pair leads one to the contradiction that

$$E_1 + E_2 < E_1 + E_2\,, \tag{2.3}$$

which implies that the ground-state single-particle density is in fact uniquely defined by the external potential of the system, provided the ground state is not degenerate, which is not a serious constraint for practical applications.

It is shown in [3] that the ground state energy, written as a functional of the density, assumes its minimum for the correct density, constrained by normalization. It is then possible to apply variational principle and find the density for any given external potential.

Since the establishment of this powerful tool, extensions in various aspects are proposed (see [4] and references therein for a review). The work in treating SM are of particular interest to us, due to the spin-dependent nature of the magnetic dipole-dipole interaction. Besides the single-particle density, another function, be it the magnetic moment density in [4], or in our case the spin-imbalance density, is needed as the variable function, over which the minimization of ground-state energy should be done.

Chapter 3

The spin-polarized case in 2D

In this section, we briefly review the results presented in the candidate's BSc thesis [7] which deals with a SP system.

3.1 Into the flatland

In order to properly handle the 2D functionals, some careful consideration is necessary, as the density functionals for a system with dipole-dipole interaction are well known in 3D [8], but display no obvious dependence on the dimensionality.

We consider here a stiff harmonic trapping potential in the z-direction with trapping frequency ω_z, so that at $T = 0$K the system remains in the axial ground state, giving rise to a factorizable Gaussian dependence in both z and p_z in the Wigner function,

$$\nu(\mathbf{r}, \mathbf{p}) = \nu_\perp(\mathbf{r}_\perp, \mathbf{p}_\perp) 2 \exp\left(-\frac{z^2}{l_z^2} - \frac{p_z^2 l_z^2}{\hbar^2}\right), \tag{3.1}$$

where $l_z = \sqrt{\hbar/(M\omega_z)}$ is the harmonic oscillator length scale in the z-direction, the numerical factor of 2 is needed for normalization, and the subscript '$_\perp$' indicates that these various quantities live in the transverse xy-plane. Although the limit of $\omega_z \to \infty$ is taken for mathematical convenience whenever possible, ω_z should be regarded as a large but finite number for a realistic situation, and the condition $\hbar\omega_z \gg k_B T$ should be

satisfied in order to achieve a 2D geometry for the system of ultra-cold atoms that we have in mind.

Correspondingly, the densities in 3D and those in 2D are related by

$$
\begin{aligned}
n^{(1)}(\mathbf{r}';\mathbf{r}'') &= n_{\perp}^{(1)}(\mathbf{r}'_{\perp};\mathbf{r}''_{\perp})\,\frac{1}{l_z\sqrt{\pi}}\exp\left[-\frac{4z_+^2+z_-^2}{4l_z^2}\right],\\
n(\mathbf{r}) &= n_{\perp}(\mathbf{r}_{\perp})\,\frac{1}{l_z\sqrt{\pi}}\exp\left[-\frac{z^2}{l_z^2}\right],\\
\rho(\mathbf{p}) &= \rho_{\perp}(\mathbf{p}_{\perp})\,\frac{l_z}{\hbar\sqrt{\pi}}\exp\left[-\frac{p_z^2 l_z^2}{\hbar^2}\right],
\end{aligned}
\tag{3.2}
$$

where $z_+ = \frac{1}{2}(z'+z'')$, $z_- = z'-z''$, such that the 2D densities and Wigner function are related in a similar manner as their 3D counter parts,

$$
\begin{aligned}
n_{\perp}^{(1)}(\mathbf{r}'_{\perp};\mathbf{r}''_{\perp}) &= \int\frac{(d\mathbf{p}_{\perp})}{(2\pi\hbar)^2}\,\nu_{\perp}\big(\tfrac{\mathbf{r}'_{\perp}+\mathbf{r}''_{\perp}}{2},\mathbf{p}_{\perp}\big)\;e^{i\mathbf{p}_{\perp}\cdot(\mathbf{r}'_{\perp}-\mathbf{r}''_{\perp})/\hbar},\\
n_{\perp}(\mathbf{r}_{\perp}) &= \int\frac{(d\mathbf{p}_{\perp})}{(2\pi\hbar)^2}\,\nu_{\perp}(\mathbf{r}_{\perp},\mathbf{p}_{\perp}),\\
\rho_{\perp}(\mathbf{p}_{\perp}) &= \int\frac{(d\mathbf{r}_{\perp})}{(2\pi\hbar)^2}\,\nu_{\perp}(\mathbf{r}_{\perp},\mathbf{p}_{\perp}),
\end{aligned}
\tag{3.3}
$$

and are normalized to the number of particles,

$$
N = \int(d\mathbf{r}_{\perp})\,n_{\perp}(\mathbf{r}_{\perp}) = \int(d\mathbf{p}_{\perp})\,\rho_{\perp}(\mathbf{p}_{\perp}). \tag{3.4}
$$

3.2 Thomas-Fermi-Dirac approximation

To evaluate the density functionals, further assumptions about the 2D Wigner function and two-body density matrix are necessary. In the spirit of the approach that was pioneered by Thomas [9], Fermi [10], and Dirac [11], a two-fold semiclassical approximation is employed here. First, $n^{(2)}$ is replaced by products of $n^{(1)}$ factors (due to Dirac) according

to

$$
\begin{aligned}
& n^{(2)}(\mathbf{r}_1', \mathbf{r}_2'; \mathbf{r}_1'', \mathbf{r}_2'') \\
&= n^{(1)}(\mathbf{r}_1'; \mathbf{r}_1'') n^{(1)}(\mathbf{r}_2'; \mathbf{r}_2'') - n^{(1)}(\mathbf{r}_1'; \mathbf{r}_2') n^{(1)}(\mathbf{r}_2''; \mathbf{r}_1''), \\
&= \frac{1}{l_z^2 \pi} \, e^{-\frac{4z_+^2 + z_-^2}{2l_z^2}} \Big(n_\perp^{(1)}(\mathbf{r}_{1\perp}'; \mathbf{r}_{1\perp}'') n_\perp^{(1)}(\mathbf{r}_{2\perp}'; \mathbf{r}_{2\perp}'') - n_\perp^{(1)}(\mathbf{r}_{1\perp}'; \mathbf{r}_{2\perp}'') n_\perp^{(1)}(\mathbf{r}_{2\perp}''; \mathbf{r}_{1\perp}') \Big), \quad (3.5)
\end{aligned}
$$

for a SP system. Such a splitting in fact corresponds to the direct and exchange terms when evaluating the interaction energy, $E_{\rm dd}$. Second, the Wigner function is a uniform disc of a finite size (due to Thomas and Fermi (TF))

$$
\nu_\perp(\mathbf{r}_\perp, \mathbf{p}_\perp) = \eta(\, \hbar^2 4\pi n(\mathbf{r}_\perp)^2 - p_\perp^2 \,) \,, \quad (3.6)
$$

where $\eta(\ )$ is the Heaviside unit step function, the power and pre-factor of the density are determined by normalization.

3.3 The 2D functionals for a spin-polarized system

By directly evaluating the z- and p_z-integration and leaving out any additive constants that do not play a role in the dynamics of the system, we obtain

$$
\begin{aligned}
E_{\rm trap}[n] &= \int (d\mathbf{r}) \, \frac{1}{2} M\omega^2 r^2 \, n(\mathbf{r}) \,, \\
E_{\rm kin}[n] &= \int (d\mathbf{r}) \, \frac{\hbar^2}{M} \, \pi \, n(\mathbf{r})^2 \,, \\
E_{\rm dd}[n] &= \frac{\mu_0 \mu^2}{4\pi} \int (d\mathbf{r}) \left(\frac{256}{45} \sqrt{\pi} \, n(\mathbf{r})^{5/2} - \pi n(\mathbf{r}) \sqrt{-\nabla^2} \, n(\mathbf{r}) \right) \\
&\equiv E_{\rm dd}^{(1)} + E_{\rm dd}^{(2)} \,, \quad (3.7)
\end{aligned}
$$

where $\sqrt{-\nabla^2}$ is an integral operator that is given by

$$\sqrt{-\nabla^2}\, n(\mathbf{r}) = \int \frac{(d\mathbf{r}')}{(2\pi)^2}(d\mathbf{k})\, k\, e^{-i\mathbf{k}\cdot(\mathbf{r}-\mathbf{r}')} n(\mathbf{r}')\,, \tag{3.8}$$

μ_0 is the permeability of free space, and μ is the magnitude of the magnetic dipole of an atom. Note that we have left out the subscripts '$_\perp$' and will continue doing so from here onwards. It is understood that all the densities here and after refer to the 2D definition specified in Eqs. (3.1) and (3.3), and all orbital vector quantities *of the system* live in the transverse xy-plane.

As a result, the TFD approximated ground state energy is given by the sum of the terms listed in Eq. (3.7). The density that minimizes the total energy, constrained by normalization (3.4), must obey

$$\frac{2\hbar^2}{M}\pi n(\mathbf{r}) + \frac{1}{2}M\omega^2 r^2 + \frac{\mu_0\mu^2}{4\pi}\left[\frac{128}{9}\sqrt{\pi}\, n(\mathbf{r})^{3/2} - 2\pi\sqrt{-\nabla^2}\, n(\mathbf{r})\right] = \frac{1}{2}M\omega^2 R^2\,, \tag{3.9}$$

where $\frac{1}{2}M\omega^2 R^2$ is the chemical potential.

3.4 Dimensionless variables

We define the natural length scale a , the dimensionless position, $\mathbf{x}$, and density, $g(\mathbf{x})$, in accordance with

$$\begin{aligned} a &= l_0 N^{1/4}, \\ \mathbf{x} &= \frac{\mathbf{r}}{a}\,, \\ g(\mathbf{x}) &= \frac{a^2}{N}\, n(\mathbf{r})\,, \end{aligned} \tag{3.10}$$

so that the scaled density is normalized to unity. Choosing $\hbar\omega N^{3/2}$ as the energy unit, we have

$$\frac{E^{(2\mathrm{D})}_{\mathrm{TFD}}[g]}{\hbar\omega N^{3/2}} = \int (d\mathbf{x}) \left[\pi g(\mathbf{x})^2 + \frac{1}{2} x^2 g(\mathbf{x}) \right.$$
$$\left. + \epsilon N^{1/4} \left(\frac{256}{45} \sqrt{\pi}\, g(\mathbf{x})^{5/2} - N^{-1/2} \pi g(\mathbf{x}) \sqrt{-\nabla^2}\, g(\mathbf{x}) \right) \right], \tag{3.11}$$

where $-\nabla^2$ now differentiates with respect to position $\mathbf{x}$, and

$$\epsilon = \frac{\mu_0 \mu^2}{4\pi l_0^3} \Big/ (\hbar\omega) \tag{3.12}$$

is a dimensionless interaction strength that can be understood as the ratio between the interaction energy of two parallel magnetic dipoles $\boldsymbol{\mu}$ separated by $l_0 = \sqrt{\hbar/(M\omega)}$ and the transverse harmonic oscillator energy scale.

The pre-factor $N^{-1/2}$ indicates that $E^{(2)}_{\mathrm{dd}}$ is a correction to the total E_{dd} in the one-percent regime, for a modest value of $N \sim 10^4$ for typical experiments with ultra-cold atoms. Given that the TFD approximation is generally introducing errors of the order of a few percent, $E^{(2)}_{dd}$ is of a negligible size. Therefore, consistently discarding it and all other $N^{-1/2}$ terms yields

$$\epsilon N^{1/4} \frac{128}{9} \sqrt{\pi} \sqrt{g(\mathbf{x})}^{\,3} + 2\pi \sqrt{g(\mathbf{x})}^{\,2} + \frac{1}{2}(x^2 - X^2) = 0\,, \tag{3.13}$$

which can be solved *analytically*.

In Fig. 3.1, we plot the dimensionless density $g(x)$ for different values of $\epsilon N^{1/4}$. We observe that the stronger the dipole repulsion (larger ϵ), the lower the central density and the larger the radius of the cloud. This feature is reminiscent of that displayed by the condensate wave function of bosonic atoms when a repulsive contact interaction is taken into account in the mean-field formalism [12]. In contrast to the (lack of) isotropy in the spatial density of a 3D SP dipolar Bose-Einstein condensate in a spherically symmetric

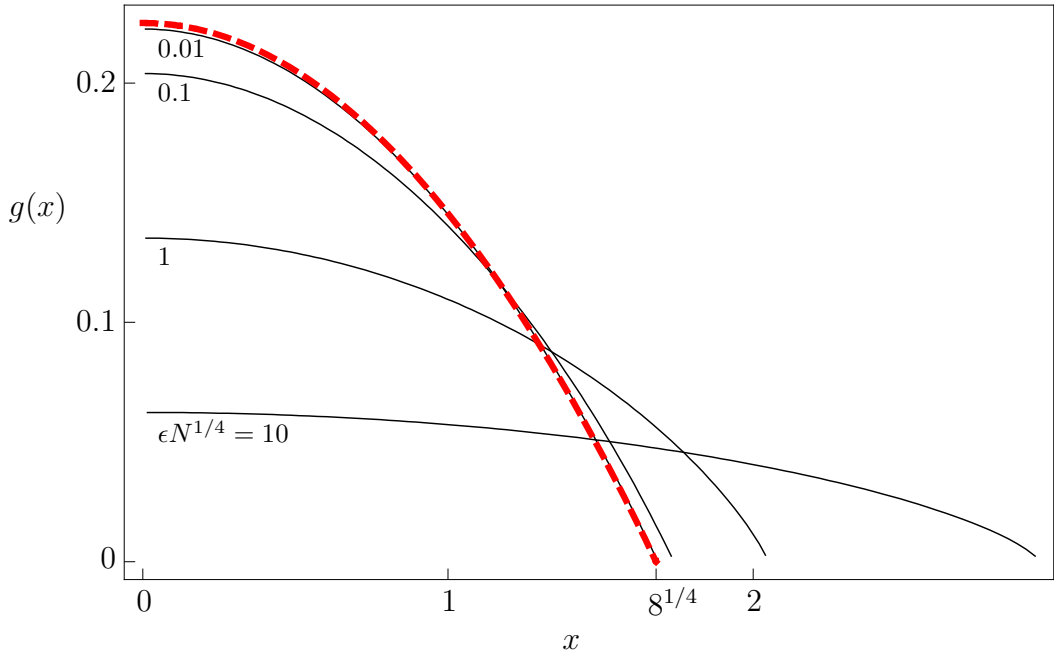

Figure 3.1: The dimensionless spatial density $g(x)$ at various values of $\epsilon N^{1/4} = 0.01, 0.1, 1, 10$ (thin lines). The TF profile (thick dashed line) is included as a reference. Note that there is an insignificant difference from the TF profile for $\epsilon N^{1/4} < 10^{-2}$.

confinement [13], the simple symmetry of the isotropic harmonic confinement is *preserved* in the ground-state density in 2D.

For weakly interacting atoms, we obtain the various contributions to the energy (in units of $\hbar\omega N^{3/2}$) up to the first order in $\epsilon N^{1/4}$,

$$E_{\rm kin} = \frac{\sqrt{2}}{3} - \frac{128}{105\pi} 2^{1/4} \epsilon N^{1/4},$$

$$E_{\rm trap} = \frac{\sqrt{2}}{3} + \frac{128}{105\pi} 2^{1/4} \epsilon N^{1/4},$$

$$E_{\rm dd}^{(1)} = \frac{512}{315\pi} 2^{1/4} \epsilon N^{1/4} \approx 0.615\, \epsilon N^{1/4}. \tag{3.14}$$

It is also possible to obtain a power law in the limit of large N, namely,

$$\begin{aligned} E_{\text{kin}} &\sim N^{7/5}\,, \\ E_{\text{trap}} &\sim N^{8/5}\,, \\ E_{\text{dd}}^{(1)} &\sim N^{8/5}\,, \\ E_{\text{dd}}^{(2)} &\sim N^{1.106}\,, \end{aligned} \tag{3.15}$$

where the final power law is obtained by a numerical fit.

Chapter 4

The spin-dependent formalism

While the above formalism yields the TFD approximated ground-state density profile and energy for a 2D cloud of spin-1/2 fermions that are polarized along the axial direction and are hence repelling each other, the lack of spherical symmetry of the magnetic-dipole interaction, which is the source of some interesting predictions such as anisotropic density in an isotropic trap [13], is not well reflected due to the peculiarity of both the configuration and the low dimension.

In order to take the spin-dependent nature of the magnetic-dipole interaction into consideration, we extend the formalism above by

1. introducing an external magnetic field strong enough to define a local quantization axis; and

2. constructing the spin-dependent Wigner functions and hence the corresponding one- and two-body spin-density matrices.

4.1 Wigner function with spin-dependence

For an arbitrary external magnetic field,

$$\mathbf{B}(\mathbf{r}) = B(\mathbf{r})\ \mathbf{e}(\mathbf{r}), \tag{4.1}$$

the magnetic energy of a single dipole is given by

$$\begin{aligned} -\mathbf{B}(\mathbf{r})\cdot\boldsymbol{\mu} &= -B(\mathbf{r})\mu\ \mathbf{e}(\mathbf{r})\cdot\boldsymbol{\sigma} \\ &\equiv -v(\mathbf{r})\ \mathbf{e}(\mathbf{r})\cdot\boldsymbol{\sigma}, \end{aligned} \tag{4.2}$$

where $\boldsymbol{\sigma}$ is the Pauli vector of a single dipole. We note that $\mathbf{B}(\mathbf{r})$ (and therefore $\mathbf{e}(\mathbf{r})$) are *external* quantities which are allowed to have the usual 3 spatial components. The TF approximated Wigner function is then a function of $\boldsymbol{\sigma}$,

$$\begin{aligned} \underline{\nu}(\mathbf{r},\mathbf{p}) &= \eta\big(-\zeta-\tfrac{p^2}{2M}-V(\mathbf{r})+v(\mathbf{r})\ \mathbf{e}(\mathbf{r})\cdot\boldsymbol{\sigma}\big) \\ &= \frac{1+\mathbf{e}(\mathbf{r})\cdot\boldsymbol{\sigma}}{2}\eta\big(P_+(\mathbf{r})-p\big)+\frac{1-\mathbf{e}(\mathbf{r})\cdot\boldsymbol{\sigma}}{2}\eta\big(P_-(\mathbf{r})-p\big), \end{aligned} \tag{4.3}$$

with

$$P_\pm(\mathbf{r}) = \big[2M\big(-\zeta-V(\mathbf{r})\pm v(\mathbf{r})\big)\big]^{1/2}, \tag{4.4}$$

and $-\zeta$ is the chemical potential. The underscore is a reminder that this Wigner function is 2×2-matrix valued. We remark that the second equality in Eq. (4.3) makes use of the fact that any function of $\boldsymbol{\sigma}$, however complicated, can always be regarded as a linear function of $\boldsymbol{\sigma}$. A quick comparison with Eq. (3.6) reveals a simple interpretation of the spin-dependent TF approximation of the Wigner function: there are two uniform discs of generally unequal size in the phase space now, each associated with one spin orientation; the radius of each disc is given in Eq. (4.4). In the event of a fully polarized cloud, $P_-(\mathbf{r})=0$, and a single disc as in Eq. (3.6) is recovered. In the opposite limit, we have $P_+(\mathbf{r})=P_-(\mathbf{r})$ for a balanced mixture, and the two discs coincide.

Now we can obtain the single-particle density with a corresponding spin dependence,

$$\begin{aligned} \underline{n}(\mathbf{r}) &= \frac{1+\mathbf{e}(\mathbf{r})\cdot\boldsymbol{\sigma}}{2}\Big(\frac{P_+(\mathbf{r})}{2\pi\hbar}\Big)^2\pi+\frac{1-\mathbf{e}(\mathbf{r})\cdot\boldsymbol{\sigma}}{2}\Big(\frac{P_-(\mathbf{r})}{2\pi\hbar}\Big)^2\pi \\ &\equiv \tfrac{1}{2}\big(n(\mathbf{r})+s(\mathbf{r})\mathbf{e}(\mathbf{r})\cdot\boldsymbol{\sigma}\big), \end{aligned} \tag{4.5}$$

with the total density $n(\mathbf{r})$ and spin-imbalance density $s(\mathbf{r})$ given by

$$n(\mathbf{r}) = \pi\left(\left(\frac{P_+(\mathbf{r})}{2\pi\hbar}\right)^2 + \left(\frac{P_-(\mathbf{r})}{2\pi\hbar}\right)^2\right),$$
$$s(\mathbf{r}) = \pi\left(\left(\frac{P_+(\mathbf{r})}{2\pi\hbar}\right)^2 - \left(\frac{P_-(\mathbf{r})}{2\pi\hbar}\right)^2\right). \tag{4.6}$$

We observe that these two functions must obey

$$|s(\mathbf{r})| \leq n(\mathbf{r}), \tag{4.7}$$

but are otherwise independent of each other. Therefore, the minimization to achieve the ground-state energy has to be done over both functions under the constraint of normalization and Eq. (4.7).

4.2 Extending Dirac's approximation

Before we proceed to derive the density functionals, it is necessary to extend Dirac's approximation, Eq. (3.5), into the corresponding spin-dependent form, $\underline{\underline{n}}^{(2)}(\mathbf{r}', \mathbf{r}''; \mathbf{r}', \mathbf{r}'')$, which is required in the evaluation of $E_{\rm dd}$. We assume that the ground-state many-body wave function of a N-fermion system can be written as a single Slater determinant,

$$\psi(r_1, \cdots, r_N) = \frac{1}{\sqrt{N!}} \det_{m,l}\left[\phi_m(r_l)\right], \tag{4.8}$$

where

$$\phi_m(r_j) = \begin{pmatrix} \alpha_m(\mathbf{r}_j) \\ \beta_m(\mathbf{r}_j) \end{pmatrix} \tag{4.9}$$

denotes a single-particle orbital with two spin components α_m and β_m, $\mathbf{r}_j$ is a 2D position variable, while r_j refers to the combination of the position and spin variables, so that $\int dr_j$ symbolically means summing over the jth spin variable *and* integrating the jth

position variable.

When expressing the one- and two-body spin-density matrices in terms of the single particle orbitals, we get

$$
\begin{aligned}
\underline{n}(\mathbf{r}';\mathbf{r}'') &= N\int dr_2\cdots dr_N\ \psi(r',r_2,\cdots,r_N)\ \psi^*(r'',r_2,\cdots,r_N) \\
&= \sum_m \begin{pmatrix} \alpha_m(\mathbf{r}')\alpha_m^*(\mathbf{r}'') & \alpha_m(\mathbf{r}')\beta_m^*(\mathbf{r}'') \\ \beta_m(\mathbf{r}')\alpha_m^*(\mathbf{r}'') & \beta_m(\mathbf{r}')\beta_m^*(\mathbf{r}'') \end{pmatrix} \\
&\equiv \begin{pmatrix} n_{\uparrow\uparrow}(\mathbf{r}';\mathbf{r}'') & n_{\uparrow\downarrow}(\mathbf{r}';\mathbf{r}'') \\ n_{\downarrow\uparrow}(\mathbf{r}';\mathbf{r}'') & n_{\downarrow\downarrow}(\mathbf{r}';\mathbf{r}'') \end{pmatrix}, \\
\underline{\underline{n}}^{(2)}(\mathbf{r}'_1,\mathbf{r}'_2;\mathbf{r}''_1,\mathbf{r}''_2) &= \frac{N(N-1)}{2}\int dr_3\cdots dr_N\ \psi(r'_1,r'_2,r_3,\cdots,r_N)\psi^*(r''_1,r''_2,r_3,\cdots,r_N) \\
&= \frac{1}{2}\sum_{l,m} \begin{pmatrix} \alpha_l(\mathbf{r}'_1) \\ \beta_l(\mathbf{r}'_1) \end{pmatrix} \otimes \begin{pmatrix} \alpha_m(\mathbf{r}'_2) \\ \beta_m(\mathbf{r}'_2) \end{pmatrix} \left[\begin{pmatrix} \alpha_l(\mathbf{r}''_1) \\ \beta_l(\mathbf{r}''_1) \end{pmatrix} \otimes \begin{pmatrix} \alpha_m(\mathbf{r}''_2) \\ \beta_m(\mathbf{r}''_2) \end{pmatrix} \right. \\
&\qquad \left. - \begin{pmatrix} \alpha_m(\mathbf{r}''_1) \\ \beta_m(\mathbf{r}''_1) \end{pmatrix} \otimes \begin{pmatrix} \alpha_l(\mathbf{r}''_2) \\ \beta_l(\mathbf{r}''_2) \end{pmatrix} \right]^\dagger \\
&= \frac{1}{2}\left(\underline{n}(\mathbf{r}'_1;\mathbf{r}''_1)\otimes\underline{n}(\mathbf{r}'_2;\mathbf{r}''_2) - \left[\underline{n}(\mathbf{r}'_1;\mathbf{r}''_2)\otimes\underline{n}(\mathbf{r}'_2;\mathbf{r}''_1)\right]_{\mathrm{T}_{23}} \right), \qquad (4.10)
\end{aligned}
$$

where the subscript '$_{\mathrm{T}_{23}}$' means interchanging the second and the third columns. The double summation in $\underline{\underline{n}}^{(2)}$ includes the self-energy, which has equal contributions to the direct and exchange terms and hence does not contribute to the sum. We remark that strictly speaking, this extension should have been in 3D, just as the original work by Dirac. However, since we consider a system in the axial ground state, Eq. (4.10) is also valid in 2D, with an exponential pre-factor that depends on z' and z'', just as that in the lower line of Eq. (3.5), to be integrated with the relevant z-dependence in the interaction

potential. Note that the surviving factor is of significance in the contact interaction.

4.3 The spin-density functionals

With Eq. (4.5), we can evaluate the trap and magnetic energy directly,

$$\begin{aligned}
E_{\text{trap}} &= \text{tr}_{2\times 2} \int (d\mathbf{r})\ \tfrac{1}{2} M\omega^2 r^2\ \underline{n}(\mathbf{r}) \\
&= \int (d\mathbf{r})\ \tfrac{1}{2} M\omega^2 r^2\ \text{tr}_{2\times 2}\ \underline{n}(\mathbf{r}) \\
&= \int (d\mathbf{r})\ \tfrac{1}{2} M\omega^2 r^2\ n(\mathbf{r}), \\
E_{\text{mag}} &= \text{tr}_{2\times 2} \int (d\mathbf{r})\ (-\boldsymbol{\mu})\cdot \mathbf{B}(\mathbf{r})\ \underline{n}(\mathbf{r}) \\
&= -\int (d\mathbf{r})\ v(\mathbf{r})\ \text{tr}_{2\times 2}\ \mathbf{e}(\mathbf{r})\cdot \boldsymbol{\sigma}\ \underline{n}(\mathbf{r}) \\
&= -\int (d\mathbf{r})\ v(\mathbf{r}) s(\mathbf{r}).
\end{aligned} \tag{4.11}$$

The evaluation of kinetic energy requires Eq. (4.3),

$$\begin{aligned}
E_{\text{kin}} &= \text{tr}_{2\times 2} \int (d\mathbf{r}) \frac{(d\mathbf{p})}{(2\pi\hbar)^2}\ \frac{p^2}{2M}\ \underline{\nu}(\mathbf{r},\mathbf{p}) \\
&= \int (d\mathbf{r}) \frac{(d\mathbf{p})}{(2\pi\hbar)^2}\ \frac{p^2}{2M}\ \text{tr}_{2\times 2}\ \underline{\nu}(\mathbf{r},\mathbf{p}) \\
&= \int (d\mathbf{r}) \frac{(d\mathbf{p})}{(2\pi\hbar)^2}\ \frac{p^2}{2M}\ \frac{1}{2}\Big(\eta(P_+(\mathbf{r})-p)+\eta(P_-(\mathbf{r})-p)\Big) \\
&= \int (d\mathbf{r}) \frac{1}{(2\pi\hbar)^2}\ \frac{\pi}{2M}\big(P_+(\mathbf{r})^4+P_-(\mathbf{r})^4\big) \\
&= \int (d\mathbf{r})\ \frac{\pi\hbar^2}{2M}\big(n(\mathbf{r})^2+s(\mathbf{r})^2\big).
\end{aligned} \tag{4.12}$$

To evaluate E_{dd}, we first observe that the dipole-dipole interaction potential is natu-

rally split into a singlet and a triplet components,

$$V_{\rm dd}(\mathbf{r}) = \frac{\mu_0}{4\pi}\,\boldsymbol{\mu}^{(1)}\cdot\Big[\underbrace{\frac{\overleftrightarrow{1}}{r^3}-3\,\frac{\mathbf{rr}}{r^5}}_{\text{triplet}}\;\underbrace{-\frac{8\pi}{3}\,\delta(\mathbf{r})\overleftrightarrow{1}}_{\text{singlet}}\Big]\cdot\boldsymbol{\mu}^{(2)}, \tag{4.13}$$

so that the singlet interaction energy can be computed by direct integration with the actual expression of $\underline{\underline{n}}^{(2)}(\mathbf{r}',\mathbf{r}'';\mathbf{r}',\mathbf{r}'')$,

$$\begin{aligned}
E_{\rm dd,s} &= {\rm tr}_{4\times4}\int(d\mathbf{r}')(d\mathbf{r}'')\,\frac{1}{l_z\sqrt{2\pi}}\,\underline{\underline{n}}^{(2)}(\mathbf{r}',\mathbf{r}'';\mathbf{r}',\mathbf{r}'')\frac{\mu_0}{4\pi}\,\boldsymbol{\mu}\cdot\Big(-\frac{8\pi}{3}\delta(\mathbf{r}'-\mathbf{r}'')\overleftrightarrow{1}\Big)\cdot\boldsymbol{\mu}\\
&= \int(d\mathbf{r}')(d\mathbf{r}'')\,\frac{1}{l_z\sqrt{2\pi}}\frac{\mu_0\mu^2}{4\pi}\Big(-\frac{8\pi}{3}\delta(\mathbf{r}'-\mathbf{r}'')\Big){\rm tr}_{4\times4}\,\boldsymbol{\sigma}\cdot\overleftrightarrow{1}\cdot\boldsymbol{\tau}\,\underline{\underline{n}}^{(2)}(\mathbf{r}',\mathbf{r}'';\mathbf{r}',\mathbf{r}'')\\
&= \frac{\sqrt{2\pi}}{l_z}\,\frac{\mu_0\mu^2}{4\pi}\int(d\mathbf{r})\,\big[n(\mathbf{r})^2-s(\mathbf{r})^2\big],
\end{aligned} \tag{4.14}$$

where the factor of $1/(l_z\sqrt{2\pi})$ originates from the z-integration while reducing the dimensionality,

$$\int dz_+dz_-\frac{1}{l_z^2\pi}\,e^{-\frac{4z_+^2+z_-^2}{2l_z^2}}\delta(z_-)=\frac{1}{l_z\sqrt{2\pi}}\,. \tag{4.15}$$

We remark that, firstly, the positive sign of the energy might be in apparent contradiction with the classical picture of two opposite dipoles attracting each other, but we need to remember that the state of two opposite dipoles is a superposition of a singlet and triplet components, and the long-range attraction is only experienced by the triplet, leaving the singlet interacting only via a repulsive contact interaction. Secondly, owing to the $1/l_z$ scaling, the relative strength of this term can be tuned by adjusting the stiffness of the z-confining trap.

On the other hand, the triplet states interact according to the remaining terms in the dipole potential. Since these states are symmetric under particle exchange, we use, instead of the $\underline{\underline{n}}^{(2)}$ in Eq. (4.10), an alternative two-body density,

$$\underline{\underline{\tilde{n}}}^{(2)}(\mathbf{r}',\mathbf{r}'';\mathbf{r}',\mathbf{r}'')=\tfrac{1}{2}\Big(\underline{n}(\mathbf{r}')\otimes\underline{n}(\mathbf{r}'')-\underline{n}(\mathbf{r}';\mathbf{r}'')\otimes\underline{n}(\mathbf{r}'';\mathbf{r}')\Big), \tag{4.16}$$

which yields the same energy but greatly simplifies the computation due to its tensor product structure. The triplet interaction energy is then given by

$$E_{\rm dd,t} = {\rm tr}_{4\times4}\frac{\mu_0\mu^2}{4\pi}\int(d\mathbf{r}')(d\mathbf{r}'')\ \frac{1}{\rho^3}\ \underline{\underline{\tilde{n}}}^{(2)}(\mathbf{r}',\mathbf{r}'';\mathbf{r}',\mathbf{r}'')\left(\boldsymbol{\sigma}\cdot\boldsymbol{\tau}-3\ \frac{\boldsymbol{\sigma}\cdot\boldsymbol{\rho}\boldsymbol{\rho}\cdot\boldsymbol{\tau}}{\rho^2}\right), \tag{4.17}$$

with $\boldsymbol{\rho}=\mathbf{r}'-\mathbf{r}''$, and $\boldsymbol{\tau}$ denotes the Pauli vector of the second atom. To evaluate this expression, we apply the same procedure as that used to obtain the third line of Eq. (3.7) and find

$$\begin{aligned}E^{(1)}_{\rm dd,t} &= \frac{32}{45}\sqrt{2\pi}\frac{\mu_0\mu^2}{4\pi}\int(d\mathbf{r})\frac{3e_z(\mathbf{r})^2-1}{2}\Big[\big(n(\mathbf{r})+s(\mathbf{r})\big)^{5/2}+\big(n(\mathbf{r})-s(\mathbf{r})\big)^{5/2}\\ &\qquad -\frac{f(\gamma)}{8}\big(n(\mathbf{r})+s(\mathbf{r})\big)^{3/2}\big(n(\mathbf{r})-s(\mathbf{r})\big)\Big],\\ E^{(2)}_{\rm dd,t} &= -\frac{1}{2}\frac{\mu_0\mu^2}{4\pi}\int(d\mathbf{r})(d\mathbf{r}')\ \frac{\nabla s_z(\mathbf{r})\cdot\nabla' s_z(\mathbf{r}')-\nabla\cdot\mathbf{s}(\mathbf{r})\nabla'\cdot\mathbf{s}(\mathbf{r}')}{|\mathbf{r}-\mathbf{r}'|},\end{aligned} \tag{4.18}$$

where $e_z(\mathbf{r})$ is the z-component of $\mathbf{e}(\mathbf{r})$, $\gamma=(P_-(\mathbf{r})/P_+(\mathbf{r}))^2$, which is essentially the ratio between the Fermi energies of the minority and majority spin components, and

$$f(\gamma)=(\gamma^{-1}+14+\gamma)E(\gamma)+(-\gamma^{-1}-6+7\gamma)K(\gamma) \tag{4.19}$$

is a combination of the complete elliptic integrals of the first kind $K(\ )$ and second kind $E(\ )$, and is smooth and finite for $0\le\gamma\le1$. We remark that by setting $\gamma=0$, we recover the $E^{(1)}_{\rm dd}$ in Eq. (3.7). It is apparent from Fig. 4.1 that within a small relative error of 0.4%, $f(\gamma)$ can be replaced by a linear function $\tilde{f}(\gamma)=\frac{15}{4}\pi+(16-\frac{15}{4}\pi)\gamma$ for simplification.

For computational convenience, we again turn to the dimensionless quantities specified

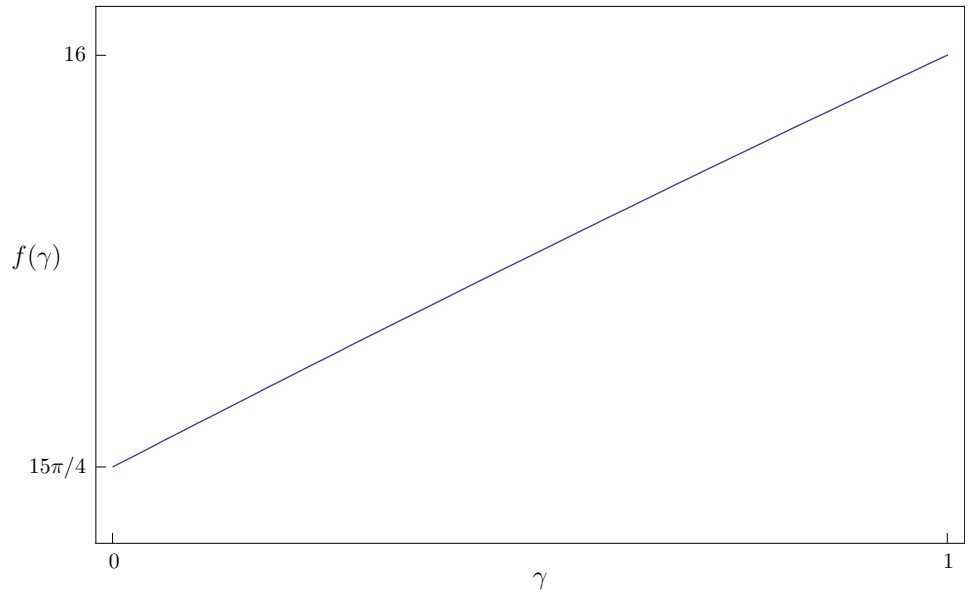

Figure 4.1: $f(\gamma)$ at relevant values of γ. It can be shown that $15\pi/4 < f(\gamma) < 16$ for $0 < \gamma < 1$.

in Eq. (3.10), with the addition of the dimensionless spin-imbalance density,

$$\begin{aligned}\mathbf{h}(\mathbf{x}) &= h(\mathbf{x})\mathbf{e}(\mathbf{x}),\\ h(\mathbf{x}) &= \frac{a^2}{N}s(\mathbf{r})\\ &\equiv \cos\big(\vartheta(\mathbf{x})\big)\ g(\mathbf{x}),\end{aligned} \tag{4.20}$$

re-parameterized so that Eq. (4.7) is automatically fulfilled. The total energy of the system is then given by

$$\begin{aligned}\frac{E^{(2\mathrm{D})}_{\mathrm{TFD}}[g,\vartheta]}{\hbar\omega N^{3/2}} = \int(d\mathbf{x})\ \Bigg[&\frac{\pi}{2}g(\mathbf{x})^2\Big(1+\cos^2\big(\vartheta(\mathbf{x})\big)\Big) + \frac{1}{2}x^2 g(\mathbf{x}) - \frac{1}{\sqrt{N}}\frac{v(\mathbf{x})}{\hbar\omega}g(\mathbf{x})\cos\big(\vartheta(\mathbf{x})\big)\\ &+ \epsilon\sqrt{\frac{\omega_z}{\omega}}\sqrt{2\pi}\,g(\mathbf{x})^2\Big(1-\cos^2\big(\vartheta(\mathbf{x})\big)\Big)\\ &+ \epsilon N^{1/4}\ \frac{3e_z(\mathbf{x})^2-1}{2}\ \frac{256}{45}\sqrt{\pi}\,g(\mathbf{x})^{5/2}\ \chi\big(\cos\big(\vartheta(\mathbf{x})\big)\big)\\ &- \epsilon N^{-1/4}\ \frac{1}{2}\int(d\mathbf{x}')\frac{\nabla h_z(\mathbf{x})\cdot\nabla' h_z(\mathbf{x}') - \nabla\cdot\mathbf{h}(\mathbf{x})\nabla'\cdot\mathbf{h}(\mathbf{x}')}{|\mathbf{x}-\mathbf{x}'|}\Bigg],\end{aligned} \tag{4.21}$$

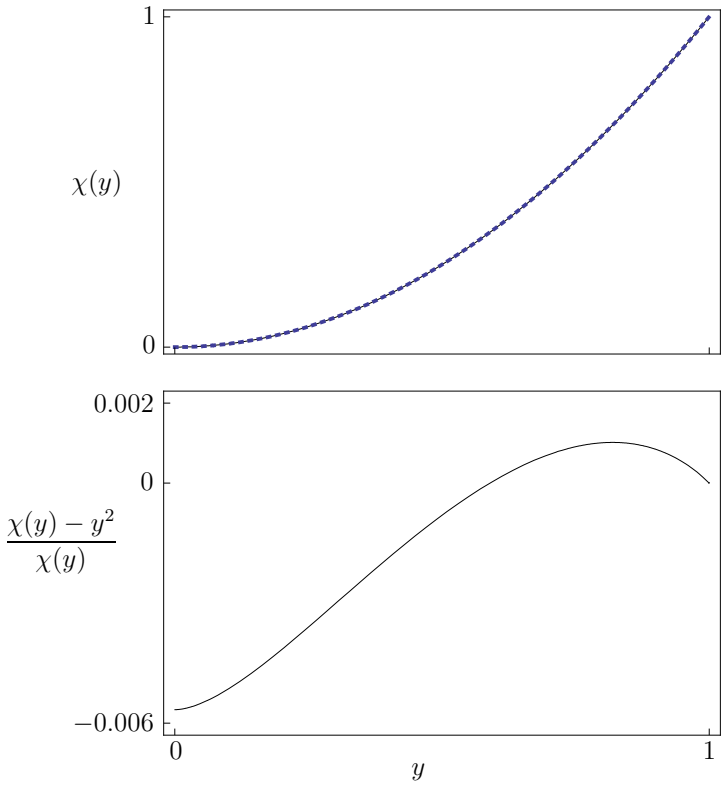

Figure 4.2: We plot $\chi(y)$ (top panel, thin solid line) in comparison with y^2 (top panel, thick dashed line) for $0 \leq y \leq 1$. The relative error of $y^2 \approx \chi(y)$ is shown in the bottom panel. It is clear that the approximation is accurate within 0.6% of the actual value of $\chi(y)$.

where

$$\chi(y) = \frac{1}{2^{5/2}} \left((1+y)^{5/2} + (1-y)^{5/2} - \frac{1}{8} f\left(\frac{1-y}{1+y}\right)(1+y)^{3/2}(1-y) \right). \tag{4.22}$$

We observe that similar to the SP case, $E^{(2)}_{\mathrm{dd,t}}$ is always a factor of $N^{-1/2}$ smaller than $E^{(1)}_{\mathrm{dd,t}}$ for $\frac{3e_z(\mathbf{x})^2-1}{2} \sim 1$, i.e. an almost normal polarization. Repeating the earlier argument used in the SP case, we consistently discard it in the following computation. In addition, numerical evidence shows that

$$\chi\big(\cos\left(\vartheta(\mathbf{x})\right)\big) \approx \cos^2\left(\vartheta(\mathbf{x})\right) \tag{4.23}$$

for all $\mathbf{x}$ within a relative error of 0.6% (see Fig. 4.2), which gives a strong justification for using this approximation.

4.4 A constant magnetic field

For a typical experiment with $N = 10^6$ atoms and a radial harmonic confinement of $\omega = 2\pi$ 20Hz, the TF radius $R_{\rm TF} = \sqrt{2}(2N)^{1/4} l_0$ is in the mm range. Hence, a uniform magnetic field throughout the extent of the cloud is feasible, so that we have

$$\begin{aligned} \mathbf{B}(\mathbf{r}) &= B_0 \mathbf{e_0}, \\ v(\mathbf{r}) &= B_0 \mu \equiv v_0. \end{aligned} \tag{4.24}$$

Applying the variational principle, we find that $g(\mathbf{x})$ and $\vartheta(\mathbf{x})$ must obey

$$g \sin\vartheta \left(A - g\cos\vartheta \Big(\pi - \epsilon \sqrt{\frac{\omega_z}{\omega}} \sqrt{8\pi} \Big) - \epsilon N^{1/4} 2 C g^{3/2} \cos\vartheta \right) = 0 \tag{4.25}$$

for unconstrained variation of ϑ, and

$$\begin{aligned} \frac{1}{2}(X^2 - x^2) = {} & g\Big(\pi + \epsilon \sqrt{\frac{\omega_z}{\omega}} \sqrt{8\pi} \Big) - \cos\vartheta \left(A - g\cos\vartheta \Big(\pi - \epsilon \sqrt{\frac{\omega_z}{\omega}} \sqrt{8\pi} \Big) \right) \\ & + \epsilon N^{1/4} \frac{5}{2} C g^{3/2} \cos^2\vartheta \end{aligned} \tag{4.26}$$

for variation of g which is normalized to unity, and the corresponding Lagrange multiplier is $\frac{1}{2}X^2$. Here we have set

$$\begin{aligned} A &= \frac{v_0}{\hbar\omega} \frac{1}{\sqrt{N}}, \\ C &= \frac{3e_{0,z}^2 - 1}{2} \frac{256}{45} \sqrt{\pi}, \end{aligned} \tag{4.27}$$

and the $\mathbf{x}$ dependence in g and ϑ is left implicit. We remark that there is no angular dependence of $\mathbf{x}$ in either (4.25) or (4.26) because we left out the integral term, which is a possible source of anisotropy intrinsic to the dipole-dipole interaction due to the gradient operators, and chose a uniform and thus isotropic magnetic field. Therefore, we expect

the solutions to be also isotropic.

We list the various solutions here[1]. First, there is a trivial solution to Eq. (4.25) for free space, $g = 0$, and $\cos\vartheta$ can be obtained from Eq. (4.26) but does not have physical meaning. Second, we have a SP solution $\sin\vartheta = 0$ from Eqs. (4.25), and (4.26) reduces to

$$\epsilon N^{1/4}\frac{128}{9}\ \frac{3e_{0,z}^2-1}{2}\sqrt{\pi}\sqrt{g}^{\,3}+2\pi\sqrt{g}^{\,2}+\frac{1}{2}(x^2-X^2)-A=0\,, \tag{4.28}$$

which is a cubic equation for $\sqrt{g}$ and can be solved analytically. Note that this further reduced to Eq. (3.13) for a normally polarized cloud, i.e. $e_{0,z} = 1$, as we expect it to do. Third, we have the SM solution, enforcing

$$A - g\cos\vartheta\Big(\pi-\epsilon\sqrt{\frac{\omega_z}{\omega}}\sqrt{8\pi}\Big)-\epsilon N^{1/4}2Cg^{3/2}\cos\vartheta=0, \tag{4.29}$$

which follows from Eq. (4.25). This is again cubic in $\sqrt{g}$ for each value of $\cos\vartheta$ (barring $\cos\vartheta = 0$, which is only possible in the complete absence of any magnetic field, i.e. $A = 0$), and establishes a complicated but nevertheless analytic relation between the two. On the other hand, the pair of (g, ϑ) can be related to the radial position x via Eq. (4.26), which is quadratic in x. However, we remind the readers that both the SP and SM solutions are approximate due to Eq. (4.23), even though the error introduced by this approximation is expected to be small. We remark that depending on the external magnetic field and interaction strength, the SM solution in the centre should be accompanied by the SP solution on the peripheral, when the density drops below a critical value such that the SM solution of Eq. (4.29) is not possible for any values of $0 \leq \cos\vartheta \leq 1$. We also remark that there is an interaction dependent threshold of the external magnetic field, beyond which the SM solution is impossible, i.e. the cloud is always polarized.

[1] which is now worked out explicitly in the Master thesis of J. Röntynen [14].

4.5 The weakly-interacting limit

For experiments with ultra-cold atoms, the magnetic-dipole interaction is typically weak. We can then neglect the interaction terms altogether, and obtain the 0^{th} order approximation via

$$\pi g + \cos\vartheta\big(\pi g\cos\vartheta - A\big) = \frac{1}{2}(X^2 - x^2),$$
$$g\sin\vartheta\big(\pi g\cos\vartheta - A\big) = 0. \tag{4.30}$$

Besides the solution for free space, the two non-trivial solutions are modified accordingly. The SP solution yield the TF profile identical to that given by the formalism for SP system (see the thick dashed curve in Fig. 3.1). The SM solution is given by

$$g = \begin{cases} \frac{1}{2\pi}(2\sqrt{1-A^2} - x^2) & 0 \le x < x_- \\ \frac{1}{2\pi}\big(A + \sqrt{1-A^2} - \frac{x^2}{2}\big) & x_- \le x \le x_+ \end{cases}, \tag{4.31}$$

together with a constant spin-imbalance density in the centre,

$$g\cos\vartheta = \frac{A}{\pi}, \tag{4.32}$$

where $x_\pm$ are the radii of the SM (lower sign) and the entire cloud (upper sign) respectively, given by

$$x_\pm = 2(\sqrt{1-A^2} \pm A). \tag{4.33}$$

A plot of the SM density with $A = 0.25$ is shown in Fig. 4.3.

However, the existence of a SM requires an extremely weak external magnetic field, such that

$$A = \frac{B_0\mu}{\hbar\omega}\frac{1}{\sqrt{N}} \le \frac{1}{\sqrt{2}}. \tag{4.34}$$

This condition arises from the positivity of the radii $x_\pm$. In usual experimental set-ups,

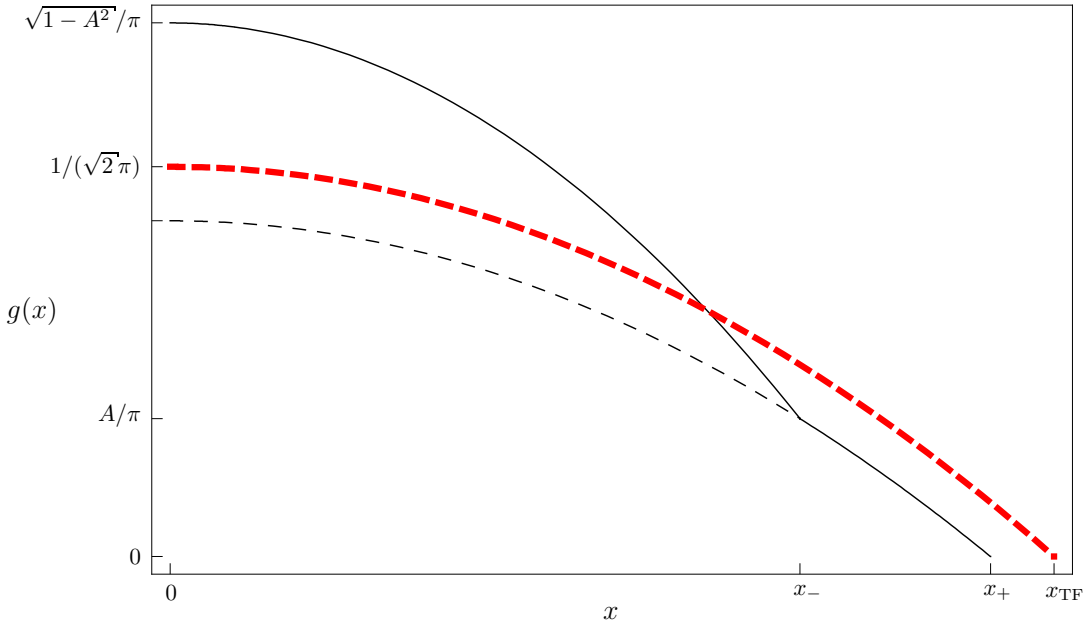

Figure 4.3: The dimensionless density profile of a SM (thin solid line) with $A = 0.25$, in comparison with the TF profile (i.e. SP solution, thick dashed line). The thin dashed line indicates the density of the majority component in the SM. For greater values of A while keeping $A \leq 1/\sqrt{2}$, the density profile approaches that of the SP solution with a lowering central density and an increasing $x_{\pm}$. In the opposite limit, we recover a mixture of equal spin-components when there is no external magnetic field, i.e. $A = 0$.

this translates into $B \sim 10$mG for a system of $N = 10^6$ atoms with a radial harmonic confinement of $\omega = 2\pi$ 20Hz. In other words, a SP cloud is readily attainable.

4.6 Arbitrary direction of polarization

So far, we have restricted our discussion to a normally polarized cloud. However, the machinery in principle allows a primitive investigation of a system with an arbitrary direction of polarization.

Naturally, we expect that only dipole-dipole interaction energy will be affected when the direction of polarization is changed. A quick look at Eq. (4.21), however indicates that, more precisely, only the triplet contribution to the interaction is affected. This can be understood by the fact that the singlet state interact only via the contact term in the dipole-dipole interaction potential, Eq. (4.13), which is independent on the orientation

of the quantization axis. For the triplet component, the magnitude of $E^{(1)}_{\mathrm{dd,t}}$ is modulated simply by the factor $\frac{3e_z(\mathrm{x})^2-1}{2}$, hence ranges from $+1$ to $-\frac{1}{2}$ times of its maximum value. On the other hand, $E^{(2)}_{\mathrm{dd,t}}$ is about a percent of maximum $E^{(1)}_{\mathrm{dd,t}}$, so that once $e_z(\mathbf{x})$ gets sufficiently small, i.e. the dipoles are aligned sufficiently close to the transverse xy-plane, the triplet interaction energy becomes negative, suggesting a collapse. In this scenario, the functional for the total energy, Eq. (4.21), is not bounded from below, indicating that further modification of the model is necessary.

On the other hand, a simple calculation of the dynamics of two classical dipoles shows the time required for two atoms under the influence of an attractive dipolar force to shorten their separation by half of its initial value, taken to be the size of the cloud, is of the order of ms. This is consistent with the collapse of dipolar Bose-Einstein Condensate of ^{53}Cr observed in [13] despite the use of a classical model. Further investigation will be of interest.

Chapter 5

Concluding remarks and outlook

We have presented the derivation of the spin-density functionals of a 2D fermionic gas of dipolar atoms under the scheme of TFD approximation. For a system with many atoms, we give analytic solution for the single-particle spatial density and spin-imbalance density, in dependence on the interaction strength and external magnetic field.

For sufficiently weak magnetic field, the system is polarized on the peripheral, but allows a SM in the centre. Depending on the strength of interaction, there exists a threshold magnetic field, beyond which the system is always polarized. With modest experimental parameter and weak interaction, the threshold magnetic field is found to be weaker than the earth's magnetic field. This suggests that in order to observe a system with SM, careful magnetic shielding is necessary.

The presence of dipole-dipole interaction generally increases the size of the system for a nearly normal polarization where the dipolar interaction is largely repulsive. However, when a polarization axis close to the transverse plane is chosen, our model fails to yield a lower bound to the total energy, indicating a collapse of the system. Further improvement to the model is necessary if one wishes to study the system in this scenario.

Having established the exact functionals, we intend to investigate the excitation energies of the system for small deviations from the equilibrium. On the other hand, it is well-known that the TF approximation is problematic at the boundary of the system. We

will follow up on the gradient corrections of von Weizsäcker type. It is perceivable that once the corrections are included, $E^{(2)}_{\mathrm{dd,t}}$ may no longer be negligible. Lastly, we would like to explore other external trapping potentials, such as anisotropic harmonic traps, possibly with an optical lattice superimposed.

Bibliography

[1] G. Grynberg, C. Robilliard, Phys. Rep. **355**, 335 (2001).

[2] V. Ahufinger *et al.*, Phys. Rev. A **72**, 063616 (2005); M. Lewenstein *et al.*, cond-mat/0606771v2 (2007).

[3] P. Hohenberg and W. Kohn, Phys. Rev. **136**, B864 (1964).

[4] R.M. Dreizler and E.K.U. Gross, *Density Functional Theory* (Springer-Verlag Berlin Heidelberg, 1990).

[5] G.A. Henderson, Phys. Rev. A **19**, 23 (1981).

[6] W. Kohn, L.J. Sham, Phys. Rev. **140**, A1133 (1965).

[7] B. Fang, *Density Functionals of a 2D Fermionic Gas in Harmonic Trap*, BSc thesis, National University of Singapore (2008).

[8] K. Góral, B.-G. Englert, and K. Rzążewski, Phys. Rev. A **63**, 033606 (2001).

[9] L.H. Thomas, Proc. Cambridge Philos. Soc. **23**, 542 (1926).

[10] E. Fermi, Rend. Lincei **6**, 602 (1927).

[11] P.A.M. Dirac, Proc. Cambridge Philos. Soc. **26**, 376 (1930).

[12] F. Dalfovo, S. Giorgini, L.P. Pitaevskii, and S. Stringari, Rev. Mod. Phys. **71**, 463 (1999).

[13] K. Góral, K. Rzążewski, and T. Pfau, Phys. Rev. A **61**, 051601(R) (2000).

[14] J. Röntynen, MSc thesis, University of Helsinki (2011).

[15] M.D. Girardeau, J. math. Phys. (N.Y.) **1**, 516 (1960).

[16] M.D. Girardeau and A. Minguzzi, Phys. Rev. Lett. **99**, 230402 (2007).

[17] T. Busch, B.-G. Englert, K. Rzążewski, and M. Wilkens, Found. Phys. **28**, 549 (1998).

[18] B. Fang, P. Vignolo, C. Miniatura, A. Minguzzi, Phys. Rev. A **79**, 023623 (2009).

[19] A. Minguzzi, Habilitation thesis, in preparation.

Appendix A

Dipole-dipole interaction in a one-dimensional spin-polarized system

For completeness, we include here the derivation of the dipole-dipole interaction energy for a one-dimensional (1D) SP system. First, we consider the reduction of dimensionality as outlined in Sec. 3.1, but now only the z- and p_z-dependence in the single-particle Wigner function is left unspecified, while in the x- and y-directions, there is a Gaussian dependence in both position and momentum, due to a stiff radial harmonic confinement. In the isotropic case, we have $\omega_x = \omega_y = \omega$, and the radial harmonic length scale is given by $l_0 = \sqrt{\hbar/(M\omega)}$, so that the Wigner function reads

$$\nu(\mathbf{r}, \mathbf{p}) = \nu_z(z, p_z) 4 \exp\left(-\frac{x^2 + y^2}{l_0^2} - \frac{(p_x^2 + p_y^2) l_0^2}{\hbar^2}\right), \tag{A.1}$$

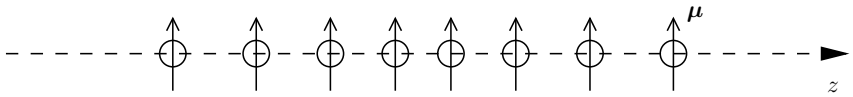

Figure A.1: An illustration of the spin orientation relative to the 1D cloud. Note that this corresponds to $\alpha = \frac{\pi}{2}$ but the choice of φ is arbitrary and does not affect our calculation.

so that the 3D and 1D single-particle densities are related by

$$\begin{aligned} n^{(1)}(\mathbf{r}';\mathbf{r}'') &= n_z^{(1)}(z';z'')\,\frac{1}{l_0^2\pi}\exp\left[-\frac{4x_+^2+x_-^2}{4l_0^2}-\frac{4y_+^2+y_-^2}{4l_0^2}\right], \\ n(\mathbf{r}) &= n_z(z)\,\frac{1}{l_0^2\pi}\exp\left[-\frac{x^2}{l_0^2}-\frac{y^2}{l_0^2}\right], \\ \rho(\mathbf{p}) &= \rho_z(p_z)\,\frac{l_0^2}{\hbar^2\pi}\exp\left[-\frac{p_x^2 l_0^2}{\hbar^2}-\frac{p_y^2 l_0^2}{\hbar^2}\right], \end{aligned} \tag{A.2}$$

where the average and difference in the x- and y-coordinates are denoted with subscripts '$_+$' and '$_-$' respectively. Applying Dirac's decomposition of two-body density matrix, we have

$$n^{(2)}(\mathbf{r}',\mathbf{r}'';\mathbf{r}',\mathbf{r}'') = \frac{1}{l_0^4\pi^2}\,e^{-\frac{4x_+^2+x_-^2}{2l_0^2}-\frac{4y_+^2+y_-^2}{2l_0^2}}\Big(n_z(z')n_z(z'')-n_z^{(1)}(z';z'')n_z^{(1)}(z'';z')\Big). \tag{A.3}$$

Since the system is spin-polarized, only the triplet terms in the dipole-dipole interaction potential (4.13) matters. By writing

$$\boldsymbol{\mu} = \mu\begin{pmatrix}\sin\alpha\cos\varphi\\ \sin\alpha\sin\varphi\\ \cos\alpha\end{pmatrix},\quad \mathbf{r} = \begin{pmatrix}\varrho\cos\phi\\ \varrho\sin\phi\\ z\end{pmatrix}, \tag{A.4}$$

and choosing a simple geometry where all dipoles are aligned perpendicular to the 1D

cloud (see Fig. A.1), the triplet interaction potential reads

$$V_{\rm dd,t}(\mathbf{r}) \;=\; \frac{\mu_0\mu^2}{4\pi}\frac{1}{(\varrho^2+z^2)^{3/2}}\Big[1-\frac{3}{\varrho^2+z^2}\Big(\varrho^2\sin^2\alpha\cos^2(\varphi-\phi) \\ +z^2\cos^2\alpha+\varrho z\sin(2\alpha)\cos(\varphi-\phi)\Big)\Big] \\ \to \frac{\mu_0\mu^2}{4\pi}\frac{1}{(\varrho^2+z^2)^{3/2}}\left(1-\frac{\frac{3}{2}\varrho^2}{\varrho^2+z^2}\right), \tag{A.5}$$

where we replaced, in the last step, the angular dependence by its average over an interval of 2π for an isotropic radial confinement. The dipole-dipole interaction energy is then given by

$$\begin{aligned} E_{\rm dd} &= \frac{1}{2}\int(d\mathbf{r})(d\mathbf{r}')\; n^{(2)}(\mathbf{r},\mathbf{r}';\mathbf{r},\mathbf{r}')V_{\rm dd,t}(\mathbf{r}-\mathbf{r}') \\ &= \frac{1}{2}\frac{\mu_0\mu^2}{4\pi}\int dx_+dy_+\Big(\frac{1}{l_0^2\pi}\Big)\; e^{-\frac{2}{l_0^2}(x_+^2+y_+^2)}\int dz\; dz'\Big(n_z(z)n_z(z')-n_z^{(1)}(z;z')n_z^{(1)}(z';z)\Big) \\ &\qquad\times\int_0^\infty \varrho d\varrho(2\pi)\;\frac{1}{l_0^2\pi}\;e^{-\varrho^2/(2l_0^2)}\left(\frac{1}{(\varrho^2+z{-}^2)^{3/2}}-\frac{\frac{3}{2}\varrho^2}{(\varrho^2+z_-^2)^{5/2}}\right) \\ &= \frac{\mu_0\mu^2}{4\pi}\int dz\; dz'\Big(n_z(z)n_z(z')-n_z^{(1)}(z;z')n_z^{(1)}(z';z)\Big) \\ &\qquad\times\frac{1}{\sqrt{2}l_0^3}\Big[(\tfrac{1}{2}+t^2)\sqrt{\pi}\,e^{t^2}\mathrm{Erfc}(t)-t\Big], \end{aligned} \tag{A.6}$$

where $t=|z-z'|/(\sqrt{2}l_0)$ is the scaled separation in the z-direction, and Erfc( ) denotes the complementary error function. We remark that for a 1D system, we need to eventually look at the $l_0\to 0^+$ limit of the expression above. However, further structure of the single-particle density and density matrix will be necessary for this purpose.

To summarize the SP case, we tabulate the density functionals of both the kinetic and dipole-dipole interaction energy in 1, 2, and 3D. It is clear that the structure of the density functionals depends crucially on the spatial dimension. The procedure used here to reduce dimensionality is by no means unique, but fairly well justified by the strong

Table A.1: Summary of the density functionals for the kinetic energy and the dipole-dipole interaction energy in 1D, 2D, and 3D. In 1D, the spins are polarized normal to the z-axis, along which the atoms align. In 2D and 3D, the spins are polarized along the z-direction, θ in 3D refers to the azimuthal angle of the vector $\mathbf{r}-\mathbf{r}'$.

	$E_{\rm kin}$	$E_{\rm dd}$
1D	$\int dz\ \frac{\pi^2\hbar^2}{6M}n(z)^3$	$\frac{\mu_0\mu^2}{4\pi}\int dz\ dz'\Big(n(z)n(z')-n(z;z')n(z';z)\Big)$ $\times\frac{1}{\sqrt{2}l_0^3}\left[\left(\frac{1}{2}+t^2\right)\sqrt{\pi}\,e^{t^2}\mathrm{Erfc}(t)-t\right]$
2D	$\int(d\mathbf{r}_\perp)\ \frac{\pi\hbar^2}{2M}n(\mathbf{r}_\perp)^2$	$\frac{\mu_0\mu^2}{4\pi}\int(d\mathbf{r}_\perp)\left[\frac{256}{45}\sqrt{\pi}\,n(\mathbf{r}_\perp)^{\frac{5}{2}}-\pi n(\mathbf{r})\sqrt{-\nabla^2}\,n(\mathbf{r}_\perp)\right]$
3D	$\int(d\mathbf{r})\ \frac{\hbar^2}{20\pi^2M}\left[6\pi^2n(\mathbf{r})\right]^{\frac{5}{3}}$	$\frac{\mu_0\mu^2}{4\pi}\int(d\mathbf{r})(d\mathbf{r}')\ \frac{1}{2}\ n(\mathbf{r})\ \frac{1-3\cos^2\theta}{\lvert\mathbf{r}-\mathbf{r}'\rvert^3}\ n(\mathbf{r}')$

confinement of a stiff harmonic trap in a possible experimental set-up.

Appendix B

A short review of concurrent works

Meanwhile, the candidate has been working on a separate project with P. Vignolo *et al* in paralell. While the subject matter does not fit into the context of density functional theory, we include a brief review of the project and results obtained without the mathematical details.

The exact solution for many-body wave function of the inhomogeneous, impenetrable Bose gas in the Tonks-Girardeau limit (infinitely strong point interaction limit) can be generalized to multi-component systems, which brings about novel issues such as spatial separation and modification of coherence properties. We consider a 1D mixture of impenetrable bosons and spin-polarized, non-interacting fermions with infinitely strong point interaction between the two species, and further assume that all particles are of equal mass and feel an identical harmonic confinement in the axial direction. The infinite interaction strength among the bosons and between the two species, together with Pauli principle, ensures that the many-body spatial wave function must vanish when any pair of coordinates takes on the same value. Under such constraints, the Fermi-Bose mapping coined by Girardeau [15] and extended to Bose-Fermi mixture by Girardeau and Minguzzi [16] gives a convenient starting point to build the ground state wave function, namely, to construct a Slater determinant of N orbitals and "repair" the symmetry properties according to the particle statistics.

With the simple and yet relatively intuitive assumption that the many-body spatial wave function is anti-symmetric only under the exchange of two fermionic coordinates[1], we construct the total wave function as the product of a Slater determinant modulus (symmetric) and an anti-symmetrizer (anti-symmetric) that impose only the fermionic anti-symmetry. The resulting wave function allows the computation of the single-particle spatial density, spatial correlation, as well as momentum distribution, for both species [18]. We found that both species have spatial density extending over the entire cloud, indicating no phase separation; the single-particle correlation is strongly modified due to interaction; the momentum distribution of the fermions, consequently, decays according to a power law at large momentum, similar to that of the Tonks-Girardeau gas.

On the other hand, the assumed symmetry under boson-fermion exchange is somewhat arbitrary in the true infinite-interaction limit. Here, the number of degenerate ground states is quantified by the number of permutations allowed and is generally large. We propose a basis for the degenerate manifold, where we sort all permutations according to the configuration [19], i.e. the relative position of the bosons and fermions, and assign a relative sign to each permutation in accordance with particle statistics, so that each state in the resulting basis is symmetric under boson-boson exchange and anti-symmetric under fermion-fermion exchange. We further propose to characterize the ground-state degeneracy at finite interaction with Young tableaux, and compute relevant quantities accordingly. This work is currently in progress and a manuscript will be prepared shortly.

[1] so that boson-fermion exchange is symmetric under our assumption, and is justified by the fact that the symmetric wave function for a two-particle problem [17] has a lower energy at large but finite interaction.